Available online at www.sciencedirect.com
ScienceDirect
International Journal of Solids and Structures 45 (2008) 1978–1992
INTERNATIONAL JOURNAL OF SOLIDS AND STRUCTURES
www.elsevier.com/locate/ijsolstr

Open-cell cellular solids: A constitutive equation for hyperelasticity with deformation induced anisotropy

P. Hård af Segerstad, S. Toll *

Department of Applied Mechanics, Chalmers University of Technology, SE-41296 Göteborg, Sweden

Received 4 December 2006; received in revised form 8 November 2007
Available online 17 November 2007

Abstract

A constitutive theory is developed for an open-cell flexible cellular solid consisting of a network of struts each connecting two vertex points. A hypothesis is proposed that vertex points move affinely in the large-deformation regime, when the struts buckle, and that the force carried by a strut is a function of the longitudinal and rotational change of its vertex-to-vertex vector. The forces consist of one longitudinal force, parallel with the vertex-to-vertex vector of the strut and one transverse force. The overall stress response is initially dominated by the longitudinal force whilst the addition of the transverse force becomes significant at large deformations. The model contains three parameters: longitudinal stiffness, bending stiffness and critical stretch of a strut. These three parameters are calibrated against a simple compression test. The model is then validated against independent experiments in a simple tension, simple shear and a combined shear-compression test on an isotropic flexible polyether urethane foam. Excellent agreement is obtained between the experiments and the model.

Keywords: Constitutive modelling; Micromechanics; Finite strains; Cellular solids; Foams

1. Introduction

Cellular solids are highly compressible materials and their stress–strain response exhibits different regimes depending on the state of volumetric deformation. One can usually identify three such regimes, denoted I, II and III in Fig. 1. In the regime I, the response is approximately linear, due to small deformations. At a critical compressive strain, individual struts begin to lose stability and buckle, whereupon their longitudinal stiffness reduces drastically. Due to elastic buckling on the micro-level, a plateau in the stress–strain response is obtained, regime II. The struts then deflect freely until neighbouring struts come into contact. The densification, regime III, initiates upon internal contact and continues towards a limiting density where the response approaches that of the homogeneous solid phase.

* Corresponding author. Tel.: +46 (0)31 7721301.
E-mail address: staffan.toll@me.chalmers.se (S. Toll).

0020-7683/$ - see front matter
doi:10.1016/j.ijsolstr.2007.11.003

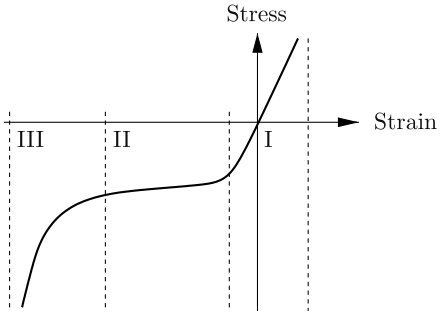

Fig. 1. Typical response to large simple compression of a hyperelastic cellular solid. I, Linear-elasticity; II, plateau; III, densification.

Micromechanical models for cellular solids typically belong to either of two categories: (i) cell-models, which consider some smallest dominant structural member of the cellular solid, e.g., one or a few struts and (ii) RVE-models, which explicitly model a representative volume element (RVE) containing a large number of struts.

Gent and Thomas (1959) developed a cell-model, category (i), based on a single-strut cell with affine motion of the strut endpoints. Their model is restricted to moderate strains since it ignores any reorientation of the microstructure. The compressive response of struts undergoing buckling was modelled in a semi-empirical manner. Zilauts and Lagzdin (1992) used a similar approach with a pin jointed single-strut, subjected to longitudinal forces, and assumed affine motion of the strut endpoints. This model allows for truly large deformations, including strut reorientation, and also incorporates a more sophisticated treatment of the response due to strut buckling. Warren and Kraynik (1991) introduced the more realistic and less restrictive assumption of affine motion of strut midpoints rather than endpoints. This allows for the non-affine stretching of a strut which is due to bending of the connecting struts. The model is more complicated than the single-strut models, since it involves solving the forces on four struts simultaneously. Only small deformations and no strut buckling are included in their analysis. Zhu et al. (1997) considered the high strain compression of open-cell foams with a body-centred-cubic (BCC) lattice where the struts are treated as built-in at rigid vertices using the *elastica* approach to model elastic buckling. It is evident that the assumption of rigid connections at the strut vertices makes the constitutive response over-stiff and that the *elastica* approach, requiring extensive iteration at the constitutive level, would be costly in a finite element method (FEM) solution scheme. Wang and Cuitiño (2000) used the same kinematic assumption as Warren and Kraynik (1991), but the solution is obtained by minimisation of energy for the unit-cell consisting of four struts. This allows the authors to examine more general configurations, although with the inherent limitation of periodicity. The most important limitation of the cell-model approach is the restrictive control of cell boundary displacements.

In RVE-models, category (ii), the balance equations on the RVE are typically solved by the FEM. Relevant background here is, e.g., Shulmeister et al. (1998), Elliott et al. (2002) and Zhu and Windle (2002), where the cellular solid is modelled as a three-dimensional framework of slender struts, regular as well as random based on the Voronoi technique. A benefit of such computations is that one may distinguish different mechanisms and study the effect of non-uniform distributions of strut parameters and connectivity. Thus, Shulmeister et al. (1998) show that Young's modulus and Poisson's ratio increase strongly with increasing disorder. Further, Van der Burg et al. (1997) conclude that, for cellular solids with higher density, the longitudinal deformation of the struts is of increasing importance relative to bending deformation. The main limitation of RVE-models is the high computational cost. Another limitation is the difficulty of choosing the appropriate boundary conditions for the RVE.

The objective of the present work is to develop a hyperelastic, constitutive equation for an open-cell cellular solid with a random microstructure. The goal is to capture the main aspects of the response at large, in particular compressive, strains: plateau behaviour due to strut buckling and deformation induced anisotropy due to strut reorientation. We propose a single-strut model, because such a model will be considerably easier to generalise for inelastic responses, is more adaptable with respect to random microstructures than multi-strut models, and is numerically less expensive. The model is based on the hypothesis that struts deform in either of

two regimes: (1) the linear small-strain regime, where the axial stiffness of a strut is much greater than the transverse stiffness, or (2) the large-strain regime, where the struts buckle so that their axial and transverse stiffness are similar. It is assumed that the struts are free to deflect between their ends; so the theory is not applicable to the densification regime, regime III in Fig. 1. It is also assumed that the micro- and macro-scales are widely separated, so that the length of a strut can be taken as infinitesimal.

2. Geometric model

The material, occupying the macroscopic (denoted by the superimposed bar) region $\overline{\Omega} \subset \mathbb{R}^3$ is on the micro-level understood to consist of two phases, one solid phase Ω_s and one pore phase Ω_p such that

$$\overline{\Omega} = \Omega_s \cup \Omega_p. \tag{1}$$

We also introduce the (undeformed) reference configuration

$$\overline{\Omega}_0 = \Omega_{s0} \cup \Omega_{p0}, \tag{2}$$

and a macroscopic, uniquely invertible, deformation map $\bar{\boldsymbol{\chi}}$:

$$\mathbf{x} = \bar{\boldsymbol{\chi}}(\mathbf{X}, t) : \overline{\Omega}_0 \to \overline{\Omega}, \tag{3}$$

see Fig. 2. The pore phase Ω_p will be assumed to have negligible stiffness in comparison to that of the solid phase Ω_s, so that its contribution to the overall stress response is ignored. The solid phase Ω_{s0} is assumed to consist of a network of struts, each connecting two vertex points $\mathbf{X}_i \in \Omega_{s0}$ and $\mathbf{X}'_i \in \Omega_{s0}$ ($i = 1 \ldots N_{\overline{\Omega}}$, where $N_{\overline{\Omega}}$ is the number of struts within the region $\overline{\Omega}$), in the reference configuration, and $\boldsymbol{\xi}_i \in \Omega_s$ and $\boldsymbol{\xi}'_i \in \Omega_s$ in the spatial configuration, see Fig. 3.

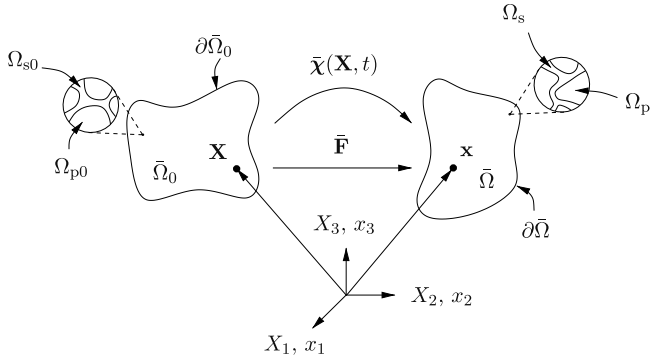

Fig. 2. General kinematics of macroscopic region $\overline{\Omega}_0$.

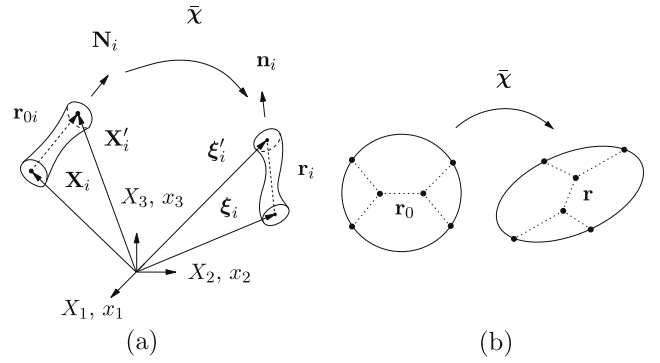

Fig. 3. (a) Affine motion of strut vertices in the large strain (post-buckling) regime, (b) illustration of affine motion for strut vertex vectors at different orientations.

As illustrated in Fig. 3, each strut i is characterised by the vertex-to-vertex vectors $\mathbf{r}_{0i}$ and $\mathbf{r}_i$ in the reference and current configurations, respectively, such that

$$\mathbf{r}_{0i} := \mathbf{X}'_i - \mathbf{X}_i = r_{0i}\mathbf{N}_i \tag{4}$$

and

$$\mathbf{r}_i := \boldsymbol{\xi}'_i - \boldsymbol{\xi}_i = r_i\mathbf{n}_i, \tag{5}$$

where $\mathbf{N}_i$ and $\mathbf{n}_i$ are the material and spatial directors of the strut, respectively, i.e., $\|\mathbf{N}_i\| = \|\mathbf{n}_i\| = 1$. For computational efficiency we now wish to link the deformation of a strut directly to the kinematics on the macroscopic level. The simplest reasonable assumption is affine motion of the vertices, cf. Fig. 3 and Zilauts and Lagzdin (1992). We shall make the following hypothesis. Regime I: in the linear elastic regime, it is well established that stretching of the (relatively stiff) struts is negligible and any deformation is dominated by transverse deflection. Thus, the affine assumption is inadequate in this regime. Nevertheless, since the strains are small we may assume that

$$\mathbf{r}_i \simeq \mathbf{r}_{0i}. \tag{6}$$

Note that although this hypothesis may hold for $\mathbf{r}_i$ itself, it does not adequately represent the infinitesimal strain in a strut. Regime II: whenever the deformations are large, the struts are in the post-buckling regime. In this regime, where the axial stiffness is governed by bending, we assume that the axial and transverse stiffness are similar, and the vertex motion is approximately affine. This implies that the motion of the vertex points is given by the macroscopic deformation map ($\bar{\boldsymbol{\chi}}$), Eq. (3),

$$\boldsymbol{\xi}_i = \bar{\boldsymbol{\chi}}(\mathbf{X}_i, t) \quad \text{such that} \quad \boldsymbol{\xi}_i \equiv \mathbf{x}_i \tag{7}$$

$$\boldsymbol{\xi}'_i = \bar{\boldsymbol{\chi}}(\mathbf{X}'_i, t) \quad \text{such that} \quad \boldsymbol{\xi}'_i \equiv \mathbf{x}'_i. \tag{8}$$

Assuming that the vertices $\mathbf{X}_i$, $\mathbf{X}'_i$ and $\mathbf{x}_i$, $\mathbf{x}'_i$ are, respectively, located within an infinitesimal distance from each other, a Taylor series expansion in the neighbourhood of $\mathbf{x}_i$ yields

$$\bar{\boldsymbol{\chi}}(\mathbf{X} + \mathbf{r}_0, t) - \bar{\boldsymbol{\chi}}(\mathbf{X}, t) = \bar{\boldsymbol{\chi}}(\mathbf{X}, t) \otimes \boldsymbol{\nabla} \cdot \mathbf{r}_0 + \mathcal{O}(r^2). \tag{9}$$

By Eqs. (4), (5), (7) and (8) the Eq. (9) is written as

$$\mathbf{r}_i \simeq \overline{\mathbf{F}} \cdot \mathbf{r}_{0i}, \tag{10}$$

where higher order terms are assumed to be negligible, since $\mathbf{r}$ is much smaller than the macroscopic dimensions (due to *separation of scales*). The dot ($\cdot$) represents a single contraction, and the macroscopic deformation gradient tensor is defined as

$$\overline{\mathbf{F}} := \bar{\boldsymbol{\chi}}(\mathbf{X}, t) \otimes \boldsymbol{\nabla} = \frac{\partial \bar{\boldsymbol{\chi}}(\mathbf{X}, t)}{\partial \mathbf{X}}. \tag{11}$$

Now since $\overline{\mathbf{F}} \simeq \bar{\mathbf{1}}$ (where $\bar{\mathbf{1}}$ is the second order identity) for small deformations, Eq. (10) *holds in both regimes* (I) and (II). In order to model the strut response in the next section, we must define objective measures of strut deformation. Assuming axisymmetry of the struts, two such measures are needed, one longitudinal and one transverse. We thus introduce the longitudinal stretch,

$$\lambda_i = \|\mathbf{r}_i\| \|\mathbf{r}_{0i}\|^{-1} = (\mathbf{N}_i \cdot \bar{\mathbf{C}} \cdot \mathbf{N}_i)^{\frac{1}{2}}, \tag{12}$$

where $\overline{\mathbf{C}} = \overline{\mathbf{F}}^{\mathrm{T}} \cdot \overline{\mathbf{F}}$ is the macroscopic right Cauchy–Green deformation tensor. The spatial director of the strut is obtained by combining Eqs. (4), (5), (10) and (12):

$$\mathbf{n}_i = \lambda_i^{-1} \overline{\mathbf{F}} \cdot \mathbf{N}_i. \tag{13}$$

To describe deflection by bending, we introduce the objective transverse deflection vector

$$\mathbf{w}_i := \mathbf{n}_i - \overline{\mathbf{R}} \cdot \mathbf{N}_i = (\lambda_i^{-1} \overline{\mathbf{F}} - \overline{\mathbf{R}}) \cdot \mathbf{N}_i, \tag{14}$$

where $\overline{\mathbf{R}}$ is the rotational part of $\overline{\mathbf{F}}$, according to the polar decomposition of the macroscopic deformation gradient, i.e., $\overline{\mathbf{F}} = \overline{\mathbf{R}} \cdot \overline{\mathbf{U}}$, and a corresponding transverse unit vector $\mathbf{t}$,

$$\mathbf{t}_i := \frac{\mathbf{w}_i}{w_i}, \tag{15}$$

with

$$w_i = \|\mathbf{w}_i\|. \tag{16}$$

The definition Eq. (14) is phenomenological, based on the idea that the rotation of vertices is defined by the rotational part of the deformation gradient (affine rotation of the vertices). The variables λ_i and w_i are non-dimensional and objective measures of longitudinal and transverse strut deformation, respectively.

3. Strut response

The force $\mathbf{f}_i$ carried by a strut cannot be modelled precisely, for the following two main reasons: (i) the geometry and boundary conditions of a strut are not well defined; (ii) the elastic solution for a strut under buckling is non-unique. However, the restriction to hyperelasticity requires $\mathbf{f}_i$ to be a unique and continuous function of $\mathbf{r}_i$. Moreover, objectivity requires the strut deformation to be independent of any rigid body rotation. We thus propose the simple deformation illustrated in Fig. 4. We must further assume the strut response to be axisymmetric, which implies that the force $\mathbf{f}_i$ is restricted to the sub space of $\mathbb{R}^3$ spanned by the vectors $\mathbf{r}_{0i}$ and $\mathbf{r}_i$, and may therefore be resolved on the two-dimensional, non-rectangular (covariant) basis $\mathbf{n}_i$, $\mathbf{t}_i$. This leads to the following form of the force acting on the strut vertex points:

$$\mathbf{f}_i = f_{\mathrm{n}}(\lambda_i, w_i)\mathbf{n}_i + f_{\mathrm{t}}(\lambda_i, w_i)\mathbf{t}_i. \tag{17}$$

In order to keep model parameters to a minimum, we presently restrict ourselves to:

$$\mathbf{f}_i = f_{\mathrm{n}}(\lambda_i)\mathbf{n}_i + f_{\mathrm{t}}(w_i)\mathbf{t}_i. \tag{18}$$

For the longitudinal response function f_{n} we assume linearity in the longitudinal stretch. Buckling under compressive load is accounted for by reducing the longitudinal stiffness below a critical stretch $\lambda < \lambda_{\mathrm{c}}$ (with $\lambda_{\mathrm{c}} < 1$):

$$f_{\mathrm{n}}(\lambda_i) = k_1(\lambda_i - 1) + (k_2 - k_1)(\lambda_i - \lambda_{\mathrm{c}})H(\lambda_i - \lambda_{\mathrm{c}}), \tag{19}$$

where $k_1 > 0$ is the tensile stiffness of the unbuckled strut, $k_2 (< k_1)$ is the reduced post-buckling stiffness and H is the Heaviside step function. For the transverse response function f_{t}, we assume linearity in w_i

$$f_{\mathrm{t}}(w_i) = k_3 w_i, \tag{20}$$

where $k_3 > 0$ is the transverse stiffness of the strut. In order to find support for the above ansatz, and to seek scaling relations between the stiffness parameters k_2 and k_3, we studied the large-deflection theory of Euler–

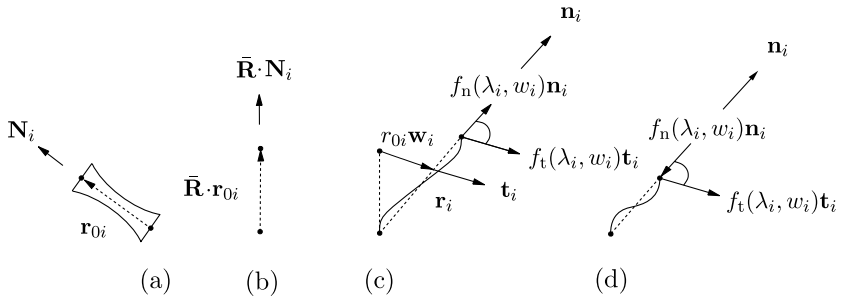

Fig. 4. Kinematics of and forces on strut vertex points in non-rectangular basis $(\mathbf{n}_i, \mathbf{t}_i)$, (––) vertex-to-vertex vector, (–) strut curvature; (a) undeformed, (b) after rigid rotation, (c) tensile stretch: $\lambda_i > 1$, (d) compressive stretch: $0 < \lambda_i < \lambda_{\mathrm{c}}$, where λ_{c} is the critical stretch at which the strut buckles. Note that $\mathbf{n}_i \cdot \mathbf{r}_i = r_i$, and that $\mathbf{n}_i \cdot \mathbf{t}_i \neq 0$ (in general).

Bernoulli beams, see Appendix A, although this theory is strictly valid only for slender beams. In the small-deflection regime, assuming the deformation mode in Fig. 4(d), one finds that k_2 as well as k_3 scale as r_0^{-2}, with the ratio

$$\frac{k_3}{k_2} = c \approx 0.55, \tag{21}$$

initially.

4. Averaging

Consider a general micro body occupying a region Ω with volume v_Ω in static equilibrium, $\boldsymbol{\sigma}\cdot\nabla = 0$, loaded by surface tractions $\mathbf{t} = \boldsymbol{\sigma}\cdot\mathbf{n}$. The average Cauchy stress within such a body is given by

$$\begin{aligned}\frac{1}{v_\Omega}\int_\Omega \boldsymbol{\sigma}\,\mathrm{d}v_\Omega &= \frac{1}{v_\Omega}\int_\Omega (\mathbf{x}\otimes\boldsymbol{\sigma})\cdot\nabla\,\mathrm{d}v_\Omega \\ &= \frac{1}{v_\Omega}\int_{\partial\Omega} (\mathbf{x}\otimes\boldsymbol{\sigma})\cdot\mathbf{n}\,\mathrm{d}s_\Omega \\ &= \frac{1}{v_\Omega}\int_{\partial\Omega} \mathbf{x}\otimes\mathbf{t}\,\mathrm{d}s_\Omega.\end{aligned} \tag{22}$$

In the case where the surface loading is concentrated to m discrete points this becomes

$$\frac{1}{v_\Omega}\int_\Omega \boldsymbol{\sigma}\,\mathrm{d}v_\Omega = \frac{1}{v_\Omega}\sum_{k=1}^{m}\mathbf{x}_k\otimes\mathbf{p}_k, \tag{23}$$

where $\mathbf{p}_k$ are point forces acting at points $\mathbf{x}_k$.

To obtain the average stress in a strut, cf. Eq. (23), we consider the free body diagram in Fig. 5(c). For simplicity, we split the strut force $\mathbf{f}_i$ into one component, $(\mathbf{f}_i\cdot\mathbf{n}_i)\mathbf{n}_i$, parallel with the strut director $\mathbf{n}_i$, and one component, $\mathbf{f}_i - (\mathbf{f}_i\cdot\mathbf{n}_i)\mathbf{n}_i = f_i^\perp\boldsymbol{\vartheta}_i$, orthogonal to $\mathbf{n}_i$ ($\|\boldsymbol{\vartheta}_i\| = 1$). Thus, applying Eq. (23), to the half-strut in Fig. 5(c) we obtain

$$\begin{aligned}\int_{\Omega_{si}}\boldsymbol{\sigma}\,\mathrm{d}v_{\Omega_{si}} &= 2\left(\frac{1}{2}\mathbf{r}_i\otimes(\mathbf{f}_i\cdot\mathbf{n}_i)\mathbf{n}_i + \frac{1}{2}\mathbf{r}_i\otimes\mathbf{f}_i^\perp + \frac{\delta}{2}\boldsymbol{\vartheta}_i\otimes\frac{r_i}{2\delta}f_i^\perp\mathbf{n}_i + \frac{\delta}{2}\boldsymbol{\vartheta}_i\otimes\frac{r_i}{2\delta}f_i^\perp\mathbf{n}_i\right) \\ &= r_i(\mathbf{n}_i\otimes\mathbf{f}_i + \mathbf{f}_i\otimes\mathbf{n}_i - (\mathbf{f}_i\cdot\mathbf{n}_i)\mathbf{n}_i\otimes\mathbf{n}_i),\end{aligned} \tag{24}$$

where δ is the (arbitrary) separation distance of the force couple acting on the vertex at the origin of the strut.

The macroscopic stress $\bar{\boldsymbol{\sigma}}$ is now obtained as the volume average of the local stress within the struts

$$\bar{\boldsymbol{\sigma}} = \frac{1}{v_{\overline{\Omega}}}\int_{\Omega_s}\boldsymbol{\sigma}\,\mathrm{d}\Omega_s = \frac{1}{v_{\overline{\Omega}}}\sum_{i=1}^{N_{\overline{\Omega}}}\int_{\Omega_{si}}\boldsymbol{\sigma}\,\mathrm{d}\Omega_{si}, \tag{25}$$

where $v_{\overline{\Omega}}$ is the volume of $\overline{\Omega}$, Ω_s is the portion of $\overline{\Omega}$ occupied by the struts and Ω_{si} is portion of Ω_s occupied by strut i. The sum is taken over all struts in $\overline{\Omega}$. Introducing Eq. (24) into Eq. (25) yields

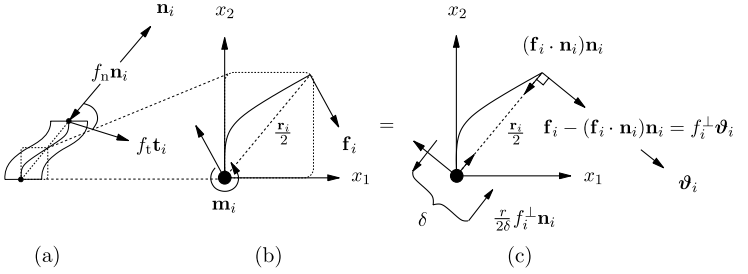

Fig. 5. (a) Forces on a strut vertex point in the non-rectangular basis $\mathbf{n}_i$, $\mathbf{t}_i$, (b) free body diagram of the half-strut, (c) free body diagram with forces resolved parallel and orthogonal to the strut director $\mathbf{n}_i$ and the couple $\mathbf{m}_i$ represented by a force couple with separation δ.

$$\bar{\boldsymbol{\sigma}} = n\langle r_i(\mathbf{n}_i \otimes \mathbf{f}_i + \mathbf{f}_i \otimes \mathbf{n}_i - (\mathbf{f}_i \cdot \mathbf{n}_i)\mathbf{n}_i \otimes \mathbf{n}_i)\rangle, \tag{26}$$

where $\langle \bullet \rangle = \frac{1}{N_{\overline{\Omega}}} \sum_{i=1}^{N_{\overline{\Omega}}} (\bullet_i)$ denotes the arithmetic average and n is the number fraction of struts, defined as

$$n := \frac{N_{\overline{\Omega}}}{v_{\overline{\Omega}}}. \tag{27}$$

Here $\overline{\Omega}$ is a representative region of the cellular solid.

Finally we assume, for simplicity, that r_0 is uniform and introduce the conservation of struts,

$$n = n_0 \overline{J}^{-1}, \tag{28}$$

where n_0 is the number fraction of struts in the reference configuration and $\overline{J} = \det(\overline{\mathbf{F}}) > 0$. The Eqs. (26) and (27) combined with Eqs. (12)–(15), (18)–(21) and (28) yield the constitutive equation

$$\bar{\boldsymbol{\sigma}} = n_0 \overline{J}^{-1} r_0 \big(\overline{\mathbf{F}} \cdot \langle \zeta \mathbf{N} \otimes \mathbf{N}\rangle \cdot \overline{\mathbf{F}}^{\mathrm{T}} - ck_2 \big(\overline{\mathbf{F}} \cdot \langle \mathbf{N} \otimes \mathbf{N}\rangle \cdot \overline{\mathbf{R}}^{\mathrm{T}} + \overline{\mathbf{R}} \cdot \langle \mathbf{N} \otimes \mathbf{N}\rangle \cdot \overline{\mathbf{F}}^{\mathrm{T}}\big)\big), \tag{29}$$

or, in terms of the second Piola–Kirchhoff stress tensor,

$$\bar{\mathbf{S}} = n_0 r_0 \big(\langle \zeta \mathbf{N} \otimes \mathbf{N}\rangle - ck_2 \big(\langle \mathbf{N} \otimes \mathbf{N}\rangle \cdot \overline{\mathbf{U}}^{-1} + \overline{\mathbf{U}}^{-1} \cdot \langle \mathbf{N} \otimes \mathbf{N}\rangle\big)\big). \tag{30}$$

Here,

$$\langle \mathbf{N}_i \otimes \mathbf{N}_i \rangle = \frac{1}{N_{\overline{\Omega}}} \sum_{i=1}^{N_{\overline{\Omega}}} \mathbf{N}_i \otimes \mathbf{N}_i, \tag{31}$$

$$\langle \zeta \mathbf{N}_i \otimes \mathbf{N}_i \rangle = \frac{1}{N_{\overline{\Omega}}} \sum_{i=1}^{N_{\overline{\Omega}}} \zeta(\lambda_i) \mathbf{N}_i \otimes \mathbf{N}_i, \tag{32}$$

with

$$\zeta(\lambda_i) = k_1 + (ck_2 - k_1)\lambda_i^{-1} + (k_2 - k_1)(1 - \lambda_c \lambda_i^{-1}) H(\lambda_i - \lambda_c) + ck_2 \lambda_i^{-2} \mathbf{N}_i \cdot \overline{\mathbf{U}} \cdot \mathbf{N}_i. \tag{33}$$

Notice that this constitutive response, Eq. (29), only depends on the initial structure and the macroscopic deformation gradient $\overline{\mathbf{F}}$. The structure tensors in Eq. (32) are evaluated from the initial orientation distribution of the struts, discretised by a set of N unit vectors $\{\mathbf{N}_i\}$. In this work we use a random orientation distribution for $\{\mathbf{N}_i\}$, thus assuming that the material is isotropic in its undeformed state.

The suitable discretisation level will be a trade-off between accuracy and CPU time efficiency. To illustrate the convergence of the overall response as the orientation discretisation is refined, Fig. 6 shows the macroscopic stress response for three different realisations using 15 (Fig. 6a), 50 (Fig. 6b), 100 (Fig. 7a) and 200 (Fig. 7b) directors, respectively. The material parameters $k_1 = 72 \times 10^{-3}$ N, $k_2 = 1.0 \times 10^{-3}$ N and ($\lambda_c = 0.974$) were used throughout. The material directors are isotropically distributed in all cases. It can be noted from Fig. 6 that about 50 strut directors seem sufficient for convergence with this method in the case of initial isotropy.

5. Experimental

A flexible polyether urethane foam with density $\rho = 26.0$ kg/m^3 was studied in order to evaluate the constitutive Eq. (29). The foam was examined by Scanning Electron Microscopy (SEM) to characterise its microstructure in both the rise and the transverse directions, respectively, see Fig. 7. The SEM photographs revealed an isotropic orientation distribution and typical strut dimensions of $r_0 = 340$ μm and $d_0 = 90$ μm, where r_0 and d_0 are the initial length and diameter, respectively.

Stress–strain data in compression, tension, simple-shear and coupled shear-compression were obtained using an apparatus developed for *soft compressible solids*, such as felts, foamed rubbers and plastics, Alkhagen and Toll (2002). In the apparatus a sample is confined between two horizontal parallel plates and deformed by imposing a vertical and/or horizontal motion on one plate relative to the other. The relative plate displacement is measured by laser sensors. The stress is measured by means of a load cell, specially designed to eliminate any influence of the free edge, see Fig. 8.

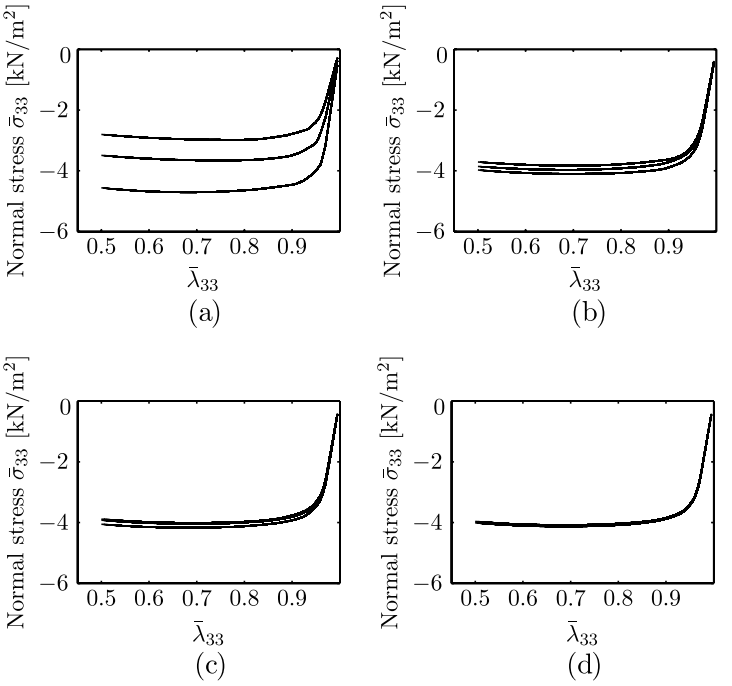

Fig. 6. Effective response. Convergence behaviour with different levels of (initially isotropic) discretisations (a) 15, (b) 50, (c) 100, (d) 200 strut directors. Each plot shows three different realisations of the discrete orientation distribution.

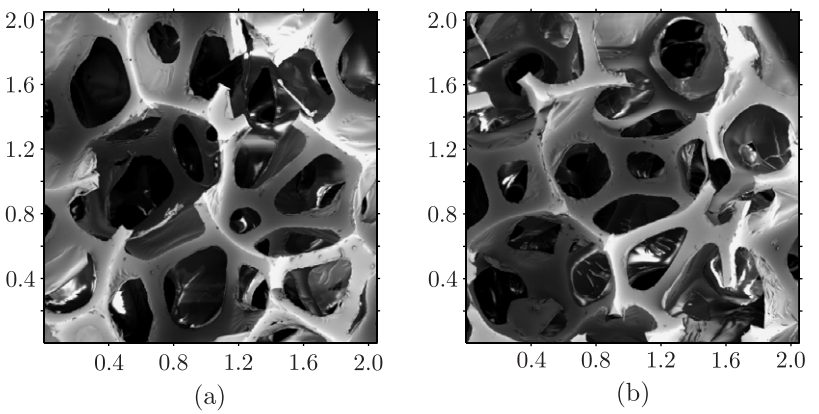

Fig. 7. Microstructure; (a) in the rise direction and (b) perpendicular to the rise direction, of the open-cell polyether urethane foam (units in mm).

The foam was cut into cylindrical specimens with different heights, $10.0 \leqslant h_0 \leqslant 25.0$ mm and diameter $d = 95.0$ mm. Prior to measurement, the specimens were cycled to eliminate the Mullin's effect, Gong et al. (2005), Holzapfel (2000), see Fig. 9, and exposed to a hysteresis loop to ensure that the dissipation was small, since we assume hyperelasticity. A hysteresis loop is shown in Fig. 10. All measurements were performed at a constant displacement rate of 0.0005 m/s to eliminate any dynamic effects, and at temperatures in the range of 20–23 °C. The humidity was also controlled but had no significant effect on the results. The model was validated against three different independent experiments: (i) simple tension, see Fig. 12, (ii) simple shear, see Fig. 13 and (iii) combined shear-compression, see Fig. 14. In the experiments (ii) and (iii), b is a displacement perpendicular to h_0. In experiment (iii) the foam was first compressed to (20%) of its initial height ($h/h_0 = 0.8$), corresponding to a point at the beginning of the plateau (regime II, Fig. 1) in the stress–strain diagram, then

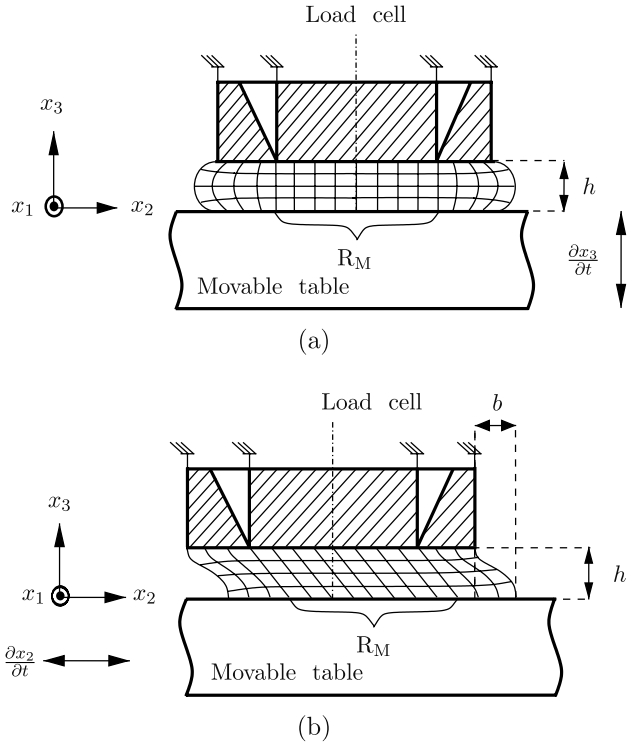

Fig. 8. Apparatus with sample deformations. The stress is measured in the undisturbed region R_M. The arrows indicate the plate motion. (a) Compression test. (b) Shear test.

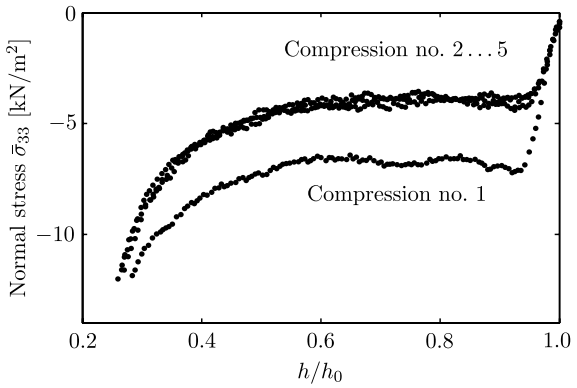

Fig. 9. Compressive stress–strain response, open-cell polyether urethane foam. The bottom curve is the first cycle and the top curves are the following cycles. (Notice that loading is from right to left.)

subjected to a simple shear deformation. In all the experiments (i), (ii), (iii), the samples were adhesively bonded to the load cell and the maximum deformation was limited by debonding between the load cell and the sample, not by densification, see Figs. 12–14.

6. Results

In the three-parameter model, k_1, k_2 and λ_c can be calibrated against a simple compression test. The parameter k_1 was adjusted to fit the slope of the response in the initial linear-elastic regime I, k_2 was used to fit the slope of the plateau regime II and λ_c was obtained from the intercept between regime I and II, see Fig. 1. The

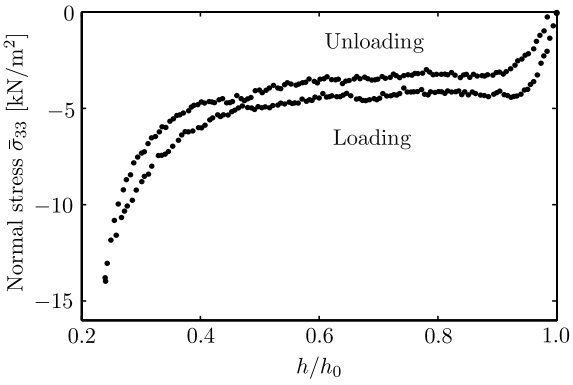

Fig. 10. Hysteresis loop, open-cell polyether urethane foam. (Notice that loading is from right to left.)

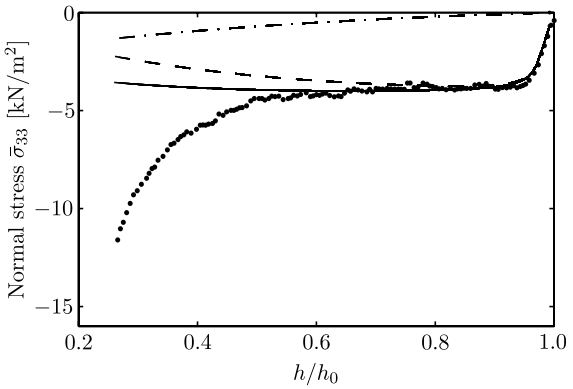

Fig. 11. Simple compression test, (–) predicted total Cauchy stress, (-·) contribution from transverse force to the Cauchy stress, (––) contribution from longitudinal force to the Cauchy stress, (···) experiment. (Notice that loading is from right to left.)

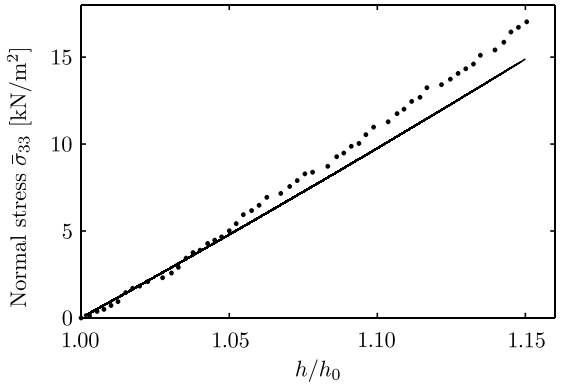

Fig. 12. Tension test, (–) predicted total Cauchy stress, (···) experiment.

resulting parameter values were $k_1 = 72 \times 10^{-3}$ N, $k_2 = 1.0 \times 10^{-3}$ N and $\lambda_c = 0.974$. In Fig. 11, the contributions from the longitudinal and transverse forces to the macroscopic Cauchy stress are plotted for a simple compression test together with the total macroscopic Cauchy stress. In Figs. 12–14, the model is validated against a simple tension, simple shear and combined shear-compression test, respectively, holding the parameters from the simple compression test, cf. Fig. 11, fixed. It may be noted that, as expected, the initial slope is the same in the compression and tension tests, compare Figs. 11 and 12. In the calibration/validation process of the model a set $\{\mathbf{N}_i\}$ of 100 initially isotropic unit vectors was used throughout.

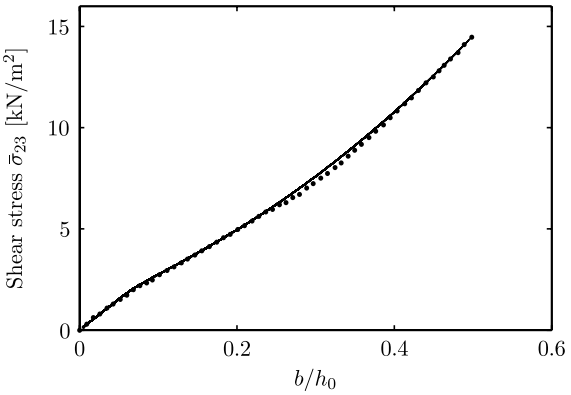

Fig. 13. Simple shear test, (–) predicted total Cauchy stress, (· · ·) experiment.

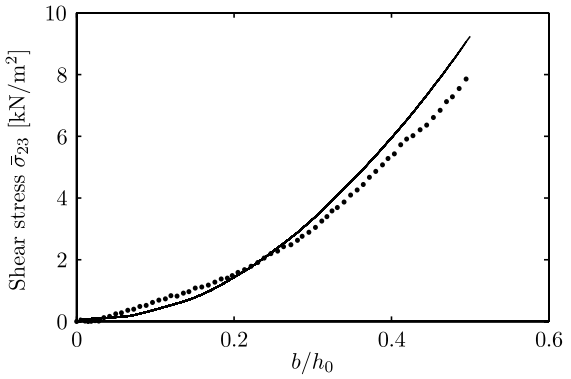

Fig. 14. Combined shear-compression test, (–) predicted total Cauchy stress, (· · ·) experiment.

7. Discussion

Clearly a general micromechanically derived constitutive theory regarding open-cell cellular solids should consider the stretching, bending and twisting of struts. The approach taken here, i.e., modelling a single strut assuming affine endpoints in the large strain regime is rather simplistic. Our reasons for this choice are that (i) it will be considerably easier to generalise to inelastic responses, which we intend to do, (ii) it is more adaptable with respect to random microstructures since the set of material directors $\{\mathbf{N}_i\}$ is easily chosen in accordance with the specific morphology of the considered foam, but also because no assumption is made with respect to the connectivity of the struts and (iii) it is computationally inexpensive as compared to multi-strut (unit-cell) or RVE models, since the equilibrium forces on the micro-level are not solved.

The non-orthogonal split of the force $\mathbf{f}$, Eq. (17), has two advantages. First, the vector $\mathbf{t}$ is considerably easier to express than a vector which is orthogonal with $\mathbf{n}$. Secondly, this choice reduces the coupling between f_n and w and f_t and λ, respectively. This happens because the transverse force due to w, $\mathbf{f}_\mathrm{t} = f_\mathrm{t}(w)\mathbf{t}$, contains a component in the direction of $\mathbf{n}$, which is consistent with the longitudinal force required to keep λ constant.

Our assumption that the stretch is close to unity in the pre-buckling regime, so that $\mathbf{r}_i \simeq \mathbf{r}_{0i}$ appears to hold. The prediction of $\mathbf{f}$ works, because the strut stiffness k_1 is adjusted to the experimental response. In the post-buckling regime, a sufficient number of members of the structure respond by bending, making their stiffness much more uniform, and the affine assumption realistic.

The hysteresis loop, see Fig. 10, shows that some energy is dissipated during the experiments. This is not taken into consideration in the *hyperelastic* constitutive model and therefore influences the values of the parameters. The average strut length $\langle r_0 \rangle$ in the model does not take into account the geometry of the vertex points, referred to as *dead volume* by Gent and Thomas (1959). The dead volumes set the boundary conditions

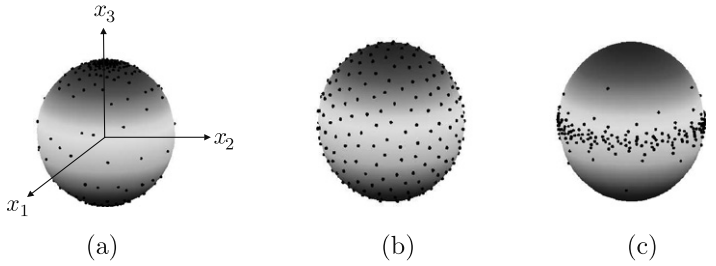

Fig. 15. Reorientation of spatial strut directors (evolution of deformation induced anisotropy) due to; (a) simple tension in the x_3 direction, (b) no deformation, (c) simple compression in the x_3 direction. The black dots represent the tips of individual directors originating at the center of the depicted unit sphere.

for the struts at the vertices and may play a significant role in especially the densification regime III which is not covered by our model. The bending of connecting struts, accounted for by Warren and Kraynik (1991), and other deformation modes, such as torsion, see Warren et al. (1997), are accommodated phenomenologically in this model by the parameters k_1 and k_2.

The consistently good predictions under different deformation modes indicate that the model decouples and captures the governing mechanisms in an adequate manner. This includes deformation induced anisotropy which is inherent in the model via the assumption of affine motion of strut vertices. Fig. 15 illustrates the distribution of spatial strut directors $\{\mathbf{n}_i\}$ as induced by simple tension, Fig. 15(a), and simple compression, Fig. 15(c). Fig. 15(b) shows the initial isotropic distribution of material strut directors $\{\mathbf{N}_i\}$.

The most remarkable ability of the model is to capture accurately the shear-compression coupling. Figs. 13 and 14 show that the shear modulus (initial slope of the solid curves) drops dramatically when the material is compressed to beyond the linear-elastic regime. This happens because a large portion of the struts in the pre-compressed material have reached their buckled state, and lost most of their stiffness. Notice that the model predicts the effect *quantitatively*, based on a calibration performed under simple compression only.

8. Conclusions

The model is based on a representation of the cellular solid by a network of struts. The forces at the vertex points are assumed to be a function of the strut deformation, which depends directly on the macroscopic deformation. The present model is formulated in terms of hyperelasticity; thus no strain rate effects or dissipation of energy are considered.

The overall stress–strain response of the cellular solid is governed primarily by longitudinal deformations of the struts including buckling. The contribution of the transverse force to the Cauchy stress is only significant at large compressive strains, where reorientation and buckling of the struts reduce the longitudinal strut response.

The model uses only three parameters, which can all be determined from a single compression test. The results of independent tests in other modes, including simple shear, are then accurately predicted. Even the peculiar shear-compression coupling is captured accurately. This strongly supports the underlying assumptions, in particular the hypothesis of affine stretch of the strut vertex-to-vertex vector at large deformations.

Acknowledgments

This work was financed by the vehicle research program (ffp) and the following participating companies: Finnveden AB, Gestamp HardTech AB, Outokumpu Stainless AB, SAAB Automobile AB, Scania CV AB, Volvo AB, Volvo Car Corporation. The authors also thank Göran Werner at Carpenter Sweden AB for supplying the foams.

Appendix A. Elastica theory

In order to support the linear ansatz (20), and reduce the number of model parameters, a scaling relation between the parameters k_2 and k_3 is sought via the large-deflection theory of slender beams. This theory is based on Newton's differential equation, obtained by combining the mathematical expression for the curvature of an analytical function, i.e.,

$$\frac{\mathrm{d}}{\mathrm{d}y}\left(\frac{\mathrm{d}u_x}{\mathrm{d}y}\right)+\kappa\left(1+\left(\frac{\mathrm{d}u_x}{\mathrm{d}y}\right)^2\right)^{\frac{3}{2}}=0, \tag{A.1}$$

with the Euler–Bernoulli beam theory,

$$\kappa=-\frac{\mathrm{d}\theta}{\mathrm{d}s}=\frac{M}{EI}. \tag{A.2}$$

Thus, let y be a coordinate along the centre-line of the beam in its material configuration, see Fig. A.1, s is a coordinate along the centre-line of the beam in its spatial configuration, u_y an axial displacement along y, u_x is a displacement orthogonal to y, $\theta(y)$ is the inclination angle at position y and EI is the flexural rigidity of the beam, Mattiasson (1979). There is no analytical solution to Eq. (A.1) but the axial displacement u_y and the transverse displacement u_x may be solved explicitly by means of elliptic integrals, see e.g., Mattiasson (1979) and Aristizábal-Ochoa (2004):

$$u_y=\frac{r_0}{2}\left(1-\frac{1}{q}[2p\sin(\varphi)\cos(\phi)+\cos(\varphi)[F(p,\phi)-K(p)+2G(p)-2G(p,\phi)]]\right), \tag{A.3}$$

$$u_x=\frac{r_0}{2}\left(\frac{1}{q}[2p\cos(\varphi)\cos(\phi)-\sin(\varphi)[F(p,\phi)-K(p)+2G(p)-2G(p,\phi)]]\right), \tag{A.4}$$

in case of a column, with unconstrained displacement in the y direction at one end, an unconstrained displacement in the x direction at the other and all other end displacements and rotations constrained. This implies that the column can be divided into two half beams according to Fig. A.1. Here

$$F(p,\phi):=\int_0^{\phi}\frac{\mathrm{d}\xi}{\sqrt{1-p^2\sin^2(\xi)}},\quad 0<p<1, \tag{A.5}$$

is the incomplete elliptic integral of the first kind,

$$G(p,\phi):=\int_0^{\phi}\sqrt{1-p^2\sin^2(\xi)}\mathrm{d}\xi,\quad 0<p<1, \tag{A.6}$$

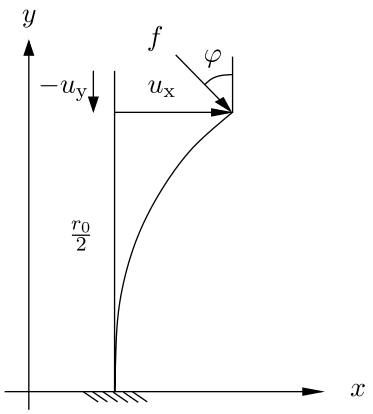

Fig. A.1. Schematic of the half-beam.

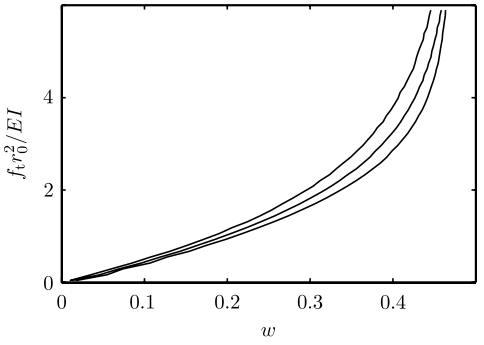

Fig. A.2. $f_t(w)$ versus w for different values of $f_n \in \{0, 0.3, 0.5\}$, where $f_n = 0.5$ is the lower curve.

is the incomplete elliptic integral of the second kind and

$$K(p) := F\left(p, \frac{\pi}{2}\right), \tag{A.7}$$

$$G(p) := G\left(p, \frac{\pi}{2}\right), \tag{A.8}$$

are the complete elliptic integrals of first and second kind, respectively. Also

$$q = \sqrt{\frac{fr_0^2}{4EI}}, \tag{A.9}$$

where f is the total applied load. Finally, φ is the angle between the load f and the y-axis, see Fig. A.1. For a prescribed value of f the iteration variable p is computed from

$$q = K(p) - F(p, \phi) \tag{A.10}$$

and

$$\phi = \arcsin\left(\frac{\sin\left(\frac{\varphi}{2}\right)}{p}\right). \tag{A.11}$$

Through a somewhat lengthy analysis of the covariant basis **n**, **t** one obtains the following relations:

$$f^2 = \left(\frac{1}{1-\frac{w^2}{4}}\right)\left(\frac{1}{1-\frac{w}{2}}f_t + \frac{w}{1-\frac{w}{2}}f_n\right)^2 + \left(\frac{1}{1-\frac{w}{2}}f_n\right)^2, \tag{A.12}$$

$$\cos\varphi = \left(\frac{1}{1-\frac{w}{2}}\right)\left(\frac{-f_n}{f}\right), \tag{A.13}$$

$$(\lambda w)^2 = u_x^2 + (u_y^2 + 1 - \lambda)^2, \tag{A.14}$$

$$\lambda^2 = u_x^2 + (u_y + 1)^2. \tag{A.15}$$

Fig. A.2 plots the solution of f_t for various constant values of f_n. It is seen that $f_t \propto w/r_0^2$ roughly up to $w \approx 0.3$.

References

Alkhagen, M., Toll, S., 2002. A triaxial rheometer for soft compressible solids. Journal of Rheology 46, 31–47.

Aristizábal-Ochoa, J.D., 2004. Large deflection stability of slender beam-columns with semirigid connections: elastica approach. Journal of Engineering Mechanics 130, 274–282.

Elliott, J.A., Windle, A.H., Hobdell, J.R., Eeckhaut, G., Oldman, R.J., Ludwig, W., Boller, E., Cloetens, P., Baruchel, J., 2002. In-situ deformation of an open-cell flexible polyurethane foam characterised by 3D computer microtomography. Journal of Materials Science 37, 1547–1555.

Gent, A.N., Thomas, A.G., 1959. The deformation of foamed elastic materials. Journal of Applied Polymer Science 1, 107–113.

Gong, L., Kyriakides, S., Jang, W.-Y., 2005. Compressive response of open-cell foams. Part I: Morphology and elastic properties. International Journal of Solids and Structures 42, 1355–1379.

Holzapfel, G.A., 2000. Nonlinear Solid Mechanics. John Wiley & Sons, Chichester, UK.

Mattiasson, K., 1979. Numerical Results from Elliptic Integral Solutions of Some Elastica Problems of Beams and Frames. Publication 79:10 Department of Structural Mechanics, Chalmers University of Technology.

Shulmeister, V., Van der Burg, M.W.D., Van der Giessen, E., Marissen, R., 1998. A numerical study of large deformations of low-density elastomeric open-cell foams. Mechanics of Materials 30, 125–140.

Van der Burg, M.W.D., Shulmeister, V., Van der Giessen, E., Marissen, R., 1997. On the linear elastic properties of regular and random open-cell foam models. Journal of Cellular Plastics 33, 31–54.

Wang, Y., Cuitiño, A.M., 2000. Three-dimensional nonlinear open-cell foams with large deformations. Journal of the Mechanics and Physics of Solids 48, 961–988.

Warren, W.E., Kraynik, A.M., 1991. The nonlinear elastic behavior of open-cell foams. Journal of Applied Mechanics 58, 376–381.

Warren, W.E., Neilsen, M.K., Kraynik, A.M., 1997. Torsional rigidity of a plateau border. Mechanics Research Communications 24, 667–672.

Zhu, H.X., Mills, N.J., Knott, J.F., 1997. Analysis of the high strain compression of open-cell foams. Journal of the Mechanics and Physics of Solids 45, 1875–1904.

Zhu, H.X., Windle, A.H., 2002. Effects of cell irregularity on the high strain compression of open-cell foams. Acta Materialia 50, 1041–1052.

Zilauts, A.F., Lagzdin, A.Zh., 1992. Single-bar model of cellular materials subjected to large elastic deformations. Mechanics of Composite Materials 28, 1–7.